ADVANCED MANEUVERING REENTRY VEHICLE INSTRUMENTATION AND COMMUNICATION TECHNIQUES

G. W. Galleher
Unit Chief
AMaRV Instrumentation and Communications

A. J. Locklair
Senior Engineer

McDonnell Douglas Astronautics Company
5301 Bolsa Avenue
Huntington Beach, CA 92647

ABSTRACT

This paper describes instrumentation and communications techniques used in the data gathering process for presently on going high performance advanced maneuvering reentry vehicle test flights.

Transducers and signal conditioning design considerations including flight test results of vibration and acoustic data (gathered simultaneously by eight FM and one 24,824 sps PCM channel), nose and control surface load cells, control actuation, flow rates, control and aerodynamic pressures, heat shield in-depth thermocouples, nose recession (nuclear and acoustic) are discussed. Also presented are the instrumentation techniques used to verify the integrity of the RF subsystem in addition to a description of the PCM, Data Delay and FM video links.

INTRODUCTION

Review of the detailed airborne instrumentation objectives for the Advanced Maneuvering Reentry Vehicle (AMaRV) flight test program indicated that packaging considerations would be a prime consideration for a successful data gathering effort. Whereas essentially no new untried instrumentation would be attempted, utilization of state of the art devices would be used and their packaging techniques improved to meet the very high environmental requirements encountered during a high performance maneuvering reentry. Performance and diagnostic measurements totaling approximately 350 analog and 400 digital (auto-pilot) were deemed necessary to verify flight test objectives. These measurements, whose PCM sampling rate varied from 8 sps to 24,824 sps also had to

utilize state-of-the-art miniaturization techniques in order to meet the very stringent volume considerations. Instrumentation hardware consisted of:

Strain Gages: Measure aerodynamic loading on the nose tip and on the control surface hinge.
Pressure Transducers: Measure vehicle body pressure loads (100 psia) and control system performance (12,000 psia).
Thermocouples: Measure heatshield performance and backface heatshield performance.
Platinum Temperature Sensors: Control system and load cell performance.
Calorimeter: Aft cover heat flux.
Thermistors: Black box temperatures.
Nuclear and Acoustic Sensors: Measure of recession.
Linear Position Transducers: Measure extension of the actuator assembly.
Piezoelectric Crystals: Measure vibration and shock environments.
Acoustic Microphones: Measure boundary layer fluctuating pressure.
Flowmeter: Measure hydraulic oil flow rates in the actuator assembly.
Directional Couplers: On-board RF performance.
Autopilot and Navigation Monitoring: Rate Gyros, Accelerometers, Inertial Platform Gyros, Guidance-Computer Parameters.
Power Distribution: Current and voltage monitors.

Additionally, included in the three vehicle flight test program are two packages classified as “piggyback” experiments. Flown on the first vehicle was a package used to measure plasma at an S-Band frequency and on the second and third vehicle is a 3 axis laser gyro and an associated guidance computer.

And also, a very significant design requirement is the specification that all flight critical units, namely the telemetry RF subsystem, the PCM, the Data Delay Unit and the centralized Signal Conditioning Unit (SCU) meet the high reliability SAMSO 73-2C Specification (parts, materials and processes).

TELEMETRY SUBSYSTEM

Figure 1 shows a block diagram of the on board data multiplexers and RF subsystem. Selection of the PCM format used for the AMaRV program was the result of tradeoffs with the following considerations:

a. Desired signal sampling rates
b. Word length and parity
c. Length of data delay (blackout) versus physical size

d. Synchronous with the on-board flight computer clock
e. Experiment capacity

A discussion of each of these follows:

Desired Sampling Rates: The most significant and by far the driving consideration regarding bandwidth utilization are the sampling rates chosen for vibration, shock and acoustic (VS&A) data. (See Figure 2). The I&C subsystem design requirement specification indicates that some data of this category must be acquired to 10 KHz. Due to size limitations and a requirement that some data must be acquired continuously, bandwidth compression techniques (on-board processor, Reference 2) are not used, but rather, the high frequency data is collected via a high sampling rate PCM and FM/FM technique. To acquire 10 KHz of VS&A data via PCM requires a minimum of 22×10^3 samples per second (SPS). Assuming a word length of 8 bits, the resulting bit rate is 166 Kbits/second per measurement. Telemetry bit rates of one megabit, though possible are not common, and would present difficulty to down-range instrumentation stations, and yet just six VS&A measurements with responses to 10 KHz would require the one megabit rate. Because of ground station recording limitation, it was concluded that the AMaRV PCM bit rate stay under 700 KHz. To accomplish this, and yet be responsive to the VS&A data, a time share technique was established. Figure 3 shows this approach. This allows one PCM channel, operating at 24,824 sps to be used. On this one PCM channel eleven VS&A measurements are time shared, i.e., one acoustic transducer is telemetered for a finite duration, it is switched off, and the next transducer output is telemetered for a short burst of time. Thus each VS&A transducer is sampled at a high sps rate, however only for short bursts. This tradeoff allows several channels to be monitored, utilizing approximately 30 to 40% of the PCM bandwidth versus using all the allowable. This approach does compromise the low frequency content of the VS&A data. Specifically, from Figure 3 an "on" time of 15.46 milliseconds allows only one sample of data at 64 hertz to be recovered whereas 150 samples of 10,000 hertz data can be recovered in the 15.46 millisecond period. The lack of low frequency data from a statistical standpoint is the problem. To compensate, several PCM channels are cross-strapped to the FM/FM telemetry link where low frequency data can be collected.

The PCM commutation scheme is also obviously invalid in assuring that shock, transient type data can be acquired on any given channel at a given time. The small 8 channel hybrid subcarrier FM system, constant 4 KHz bandwidth essentially solves this problem.

PCM channels designated at "T" are sampled at 24,824 sps and channels designated as "R" and "S" are one-half that rate. To maximize the number of on-board sensors versus allowable bandwidth, use of eight 4 KHz constant bandwidth subcarrier oscillators with a

modulation index of 1 was chosen, recognizing that high baseline noise could be expected on the subcarrier channels.

This time-shared approach leaves then approximately 400 Kbits/second of capacity for the other vehicle data.

Word Length and Parity: The resolution of the desired analog signal contributes to the overall sizing problem. An eight bit word is equivalent to one part in 256, a 10 bit word equivalent to one part in 1024. If the overall bit rate is limited to the 700K bps figure, the tradeoff is between resolution versus the number of samples. In the AMaRV PCM, an eight bit word has been chosen, modified such that five bit combinations are not used for data resolution. All zeros and all ones are not allowed, (forces a bit transition once per word), 00000001 and 00000010 are used to indicate negative over-voltage, and 11111110 indicates a positive overvoltage. The resulting resolution is one part in 250. A parity bit is also added resulting in a total word length of 9 bits. Note that the parity bit, used for an aid in data quality verification and collection requires slightly over 11% of the allowable bandwidth.

Length of Data Delay Versus Physical Size: This parameter is one of the most critical items in sizing the PCM. The maximum volume that the data delay unit can occupy is approximately 200 cubic inches. Within this volume, the maximum memory capacity is ~2.6×10^6 bits. (640 each 4K RAM's). The initial delay projected was 5 seconds. This results in a maximum bit rate, due only to the delay unit of 520 Kbit/sec. Recognizing that parity uses 11% of this, the bit rate remaining for data would be 462 Kbit/sec. VS&A data, in the time share mode, reduces the capacity for other data to 262 Kbit/sec. This value is insufficient to accommodate the required sample rates of the other vehicle subsystem telemetry requirements. Re-evaluation of the minimum acceptable delay reduced the time from 5 seconds to 3.9 seconds. Correspondingly, the maximum bit rate is: Memory size $\div$ 3.9 sec $\simeq$ 672K bit/sec.

Synchronization: This item affects the bit rate in that the clock input is derived from the on-board navigation computer. The bit rate then is not an arbitrary value, but is 7.3728 MHz divided by an integer. Resulting bit rate equals 670,254 bits/second.

Experiment Capacity: This parameter refers to sizing the PCM such that experiments as the plasma and DINS (Dormant Inertial Navigation System) can be accommmodated within the design capacity. The plasma experiment did not use any significant bandwidth, however not so with DINS (laser gyro navigation). This experiment requires bit rates of approximately 100K bits/second. This required a compromise to the VS&A data. On the second and third flights, all VS&A sample rates are reduced by one-half. The resulting PCM format is shown by Figure 4. Note that 24,824 sps for VS&A data is symetrically

cross-strapped except for word 3. Design of the PCM is such that VS&A data is actually acquired during the word 3 time slot but not inserted into the serial NRZ-L bit stream until word 4. This is due to bit sync word interference.

RF INSTRUMENTATION

As indicated by Figures 1 and 5, the telemetry subsystem requires the use of three S-band transmitters. The carrier output of these three 5 watt FM signals are multiplexed via a tuned multicavity passive device, the RF triplexer. The output port of the triplexer feeds the two vehicle telemetry antennas via a hybrid ring power divider. To measure the RF output performance of the transmitter and the antenna system, strip line directional couplers are inserted at each transmitter output as well as made integral to the hybrid ring power divider. Figures 6 and 7 show more detail of this instrumentation.

The monitor output voltages are divided down for input to 50 MV full scale differential multiplexer.

The RF antennas are detuned from free space to provide minimum mismatch (VSWR) in a plasma environment. Also two directional couplers on the antenna arms are oriented to detect RF in the reverse direction. Figure 8 shows data from a flight test. Only one of the reflected power measurements (antenna #1) is plotted, its output being nearly identical to antenna #2. The reflected power measurement indicated the onset of plasma at approximately 1657 seconds and lasting for 11 seconds. (Did not however cause blackout). Due to vehicle anomalies that caused the telemetry hardware to be exposed to mechanical environments significantly above the qualification limits, the RF transmission from two of the three links was lost at 1666 seconds. Note that as the VSMR is approaching a match condition, a slight shift, either up or down, depending on the phase angle is influencing the forward power. This plasma condition was clearly observed from the various signal strengths recorded at the down-range receivers. Various reentry experiments have been flown that measure plasma in a much more quantative manner and on AMaRV FTV-1, an AVCO package 3 was successfully flown for this purpose. The RF measurements described are packaged in a small volume, diagnostic oriented and used primarily as health checks of the RF subsystem during vehicle check-out, pre-launch and launch activities. Because of size and weight considerations, a wax pack (change of phase) heat exchanger is required to limit the temperature rise of the transmitters during ground hold and flight conditions. Note that approximately 50 watts per transmitter is dissipated as heat. Whereas an equivalent aluminum block/bulkhead interface would be 92 cubic inches, the flight wax pack occupied 37 cubic inches and weighs 1.9 pounds (0.675 pounds of tetracosane wax and 1.225 pounds of aluminum). Figure 9 shows the measured flight response of the transmitter baseplate.

VIBRATION SHOCK AND ACOUSTICS

As previously described, VS&A data was collected both on PCM and FM links. Piezoelectric crystal sensors and remotely located charge amplifiers are used to measure this environment. Due to space limitations, a very small hybrid microcircuit charge amplifier is required. This space limitation disallowed the use of a DC/DC converter such that signal ground is tied to case ground, Noise resulting from this was on the order of plus or minus one count or ±0.4% F.S. Included in the charge amplifier are aliasing filters that have a 5 pole Chebyshev response whose cut-off frequency is indicated by Figure 10. The amplifier has three pre-set gains, the selection being accomplished by external jumpering on the power/signal output connector. This feature proved quite useful in that on FTV-2 the vibration sensitivities had to be changed as the result of data acquired from the first flight. The sensor and charge amplifier are calibrated as a system at the supplier and then following installation in the vehicle, an end-to-end channel and gain verification is accomplished using the series voltage insertion method.

Figure 11 shows vibration flight data recovered from the FM/FM link and Figure 12 shows flight data from the same sensor only via the PCM/FM link in which the commutated intervals have been merged by subsequent data processing. Note the significant lower noise floor from the PCM data versus the FM data, however shock transients because of the commutation technique were, as expected, not all recovered. A one second power spectral density plot of the two approaches is shown by Figure 13 and indicates satisfactory results were obtained by the commutation method.

To measure boundary layer fluctuating pressures in a hypersonic flowfield, three acoustic microphone sensors are flown on each vehicle. The sensors are ported through the vehicle skin and heatshield via a 0.065 inch dia. hole, 0.87 inches in length. The transducers are calibrated over the expected 10 KHz frequency response range using a fixture that simulates the actual flight installation. It is recognized that the frequency response determined from an acoustical calibration in a fluid medium at rest differs significantly from the frequency response due to pressure fluctuations in a hypersonic flow field. However, acoustical calibration data can be used to estimate the sensor’s response in a hypersonic flow field. Reference 3. Figure 14 shows the results of the analysis. Modifying this roll-off is also an active 5 pole filter, cut-off at 10 KHz used to minimize aliasing errors when sampled at 24,000 sps. Figure 15 shows data recovered from FTV-2. The flight data is in good agreement with expected environment resulting from the flight trajectory.

POSITION

A variable linear displacement transducer was used to measure control surface displacement. The unit was essentially an off-the-shelf unit that was up-graded to the SAMSO 73-2C piece parts program. The output ±5 volts was fed to the SCU where it was shaped to two outputs for sampling by the PCM. One is a 0 to 5 volt signal over the full displacement range and the other a 0 to 5 volt signal over a narrow displacement range. These channels were sampled at 517 and 1034 sps respectively.

THERMAL

The thermal instrumentation flown on the AMaRV program utilizes most of the temperature sensors described in Reference 1.

In-Depth

Approximately 60 in-depth thermocouple plugs to measure heatshield performance are flown on each test flight. Each plug has 3 or 4 TC junctions (Tungsten 5% Rhenium/ Tungsten 26% Rhenium) at varying depths. See Figure 16. The resulting 190 each 45 MV F.S. measurements (5000°F) were routed directly to the low level multiplexers. These 64 channel differential multiplexers (8 bit @ 8 sps) were remotely located so as to minimize number of wires across vehicle manufacturing and field breaks. To further minimize weight and wiring complexity, all thermocouple shielding was eliminated and the cold reference junctions are in most cases simply the copper input pins on the multiplexer or in the other cases, an interconnect wire harness connector. Obviously this results in a temperature error equivalent to the uncertainty of the connector temperature which in lieu of a catastrophic heatshield failure should only be compartment temperature (~50°F). Because of variation in shingle angle θ, radius variations and depth requirements, 50 different configurations for the three flight vehicles are required. The plugs were bonded into the pre-drilled heatshield with EPON 934. Figure 17 shows typical flight data.

Backface

Chromel Alumel thermocouples, packaged in a small flexible flat pack kapton sandwich and or baynett probes also provided performance and diagnostic information of the heatshield. Approximately 25 of these sensors per vehicle were attached to the vehicle aluminum skin by sealing the kapton patch beneath a fiberglass cloth that is impregnated with EPON 934. As with the indepth thermocouples, these sensors were routed directly to the low level multiplexers.

Immersion and Black Box

Temperature measurements of on-board nitrogen and helium gas storage bottles and hydraulic oil used in the control actuation subsystem is accomplished using standard immersion probes with platinum elements. The sensors were qualified to the high environmental performance specifications (shock, vibration and acceleration). Full bridge completion networks, located in the centrally located signal conditioning unit are utilized and the sensors configured in a 3 wire connection scheme. Ten volt bridge excitation is derived in the common signal conditioning. The SCU also supplies 10 volt excitation for various thermistor networks used to monitor base plate temperatures of flight critical black boxes. Figure 18 shows the schematic and typical output of the various sensors used.

Heat Flux

In addition to the various thermal instrumentation devices described, a calorimeter was mounted on the vehicle aft cover, its output routed to a differential amplifier (gain 280) for subsequent sampling by a high level remote multiplexer.

PRESSURE TRANSDUCERS

Miniaturized solid state (piezoresistive) full bridge strain gage sensors are used to measure aerodynamic and actuator control system pressures.

Full scale for the thirteen aero sensors varies from 50 to 100 psia. Port diameter in the heat shield is 0.060 inches. The voltage output from each sensor, with 10 volt excitation is trimmed to 50 millivolts and the output applied directly to the differential input of the low level remote multiplexers. As in previous programs, plugging of the hole due to heat shield errosion occurred in several instances. However other than these few cases, good data has been recovered from all instruments to date. Figure 19 shows typical data. Eleven high pressure sensors whose range varies from 5000 to 12,000 psia are also utilized for each vehicle. The output from these sensors is also trimmed to 50 millivolts and then fed to the SCU where all eleven signals are amplified to provide a 5 volt output to the PCM. They are sampled at 500 to 1000 sps. Calibrations of the sensor and of the SCU amplifiers are merged to provide the overall system calibration with a two point actual pressure check being accomplished during vehicle bottle pressurization tests. Because of previous drift problems with the high range sensors on earlier programs, all the high range sensors (>5000 psia) are “aged” at 85% minimum F.S. pressure for a minimum of 96 hours. Calibration tests before, during and after are performed to verify acceptance and as the result, vehicle integration and flight test has revealed no problems with drift or for that matter, no flight anomalies at all with the pressure transducers have occurred.

FLOWMETER

A turbine type flowmeter is used to measure the flow rate of hydraulic oil in the control surface actuator subsystem. The requirement is to measure flow to within an accuracy of 0.6% of total usage. Trade studies indicated that an analog type tachometer signal conditioning could not meet the accuracy requirement and a circuit whose block diagram is shown by Figure 20 was designed and incorporated in the SCU. In this circuit, pulses from the flowmeter following amplification and differentiation are used to trigger a one-shot whose output feeds a divide by 16 counter. This pulse is sampled directly on a discrete (one-bit) bilevel PCM channel at 517 sps. The maximum flow rate is specified as 1700 pulses per second and hence division by 16 assures that at a 517 sample rate, the input frequency to the PCM will not exceed one-half the sample rate, Thus the maximum signal conditioning error never exceeds 16 counts over any given time interval and specifically is calculated to be 0.05%. Transducer error, primarily due to vibration and acceleration while at low flow rates resulted in 0.5% (one sigma) total error.

NOSE RECESSION

Nuclear: A significant amount of data pertaining to nosetip recession measurement has previously been presented (reference 1) and this paper will only briefly report on the AMaRV approach and results. Five radioactive Ta 182 line sources were embedded in the nosetip, the activity of each monitored by a collimated Mal gamma ray detector. Two additional detectors, which were shielded from the line sources are provided to detect any radioactive material deposited on the heatshield outer surface. The sensed gamma particles were counted by a 12 bit counter over a 62.5 millisecond time interval. The accumulated counts were D/A converted to a 5 volt signal and sampled by the PCM at 16 sps. Only 8 of the 12 bits are selected for D/A conversion, the bit positions selected is accomplished by a single jumper wire at the vehicle test connector located on the vehicle aft cover. This versatility allowed maximum resolution as a function of Ta 182 activity (half life) versus launch hold. The PCM unit supplied a synchronization pulse for a simultaneous dump and hold from all sensor counters at the end of each 62.5 millisecond period at which time all counters are reset to zero count. Valid data was recovered from this system on flights FTV-1 and FTV-2. Detailed analysis of this data is beyond the scope of this paper, suffice to say the flight data appeared to be in excellent agreement with pre-flight predictions.

Acoustic: As with the nuclear recession sensors, detailed data is also available which describes in detail, acoustic measurement devices used to obtain nosetip recession (Reference 4). A single ray device, similar to that flown on ABRV, has been selected for use on FTV-3. The unit was requalified to the higher AMaRV dynamic environmental specification. One time frame of the unit selected has 192 each 1.3 millisecond time bins (0.5 μsec each echo time). The frame will be sampled on a 1000 sps PCM channel.

SIGNAL CONDITIONING/LOAD CELLS AND CALIBRATION

Development of flight sensors to measure nose tip and control surface hinge loads was a major design effort. Concurrent with this design was the development of associated signal conditioning. In an effort to reduce package size, on-board signal conditioning associated with pressure, flow, temperature and position was combined with the load cell conditioning in a common package. A block diagram of this approach is shown by Figure 21. Note that three different and independent 10 volt regulators are utilized to supply bridge excitations and that one signal regulator is not dedicated to a particular group of sensor types, i.e., a inflight regulator failure will not cause loss of all load cell data. Note also that a DC/DC converter was not utilized because of space limitations and this gave rise to DC ground loops. Voltage offset in all SCU measurements due to this ground loop is continuously measured and telemetered throughout flight and simply subtracted from affected measurements during data processing.

Use of potentiometers to balance the load cells (strain gage bridges) were disallowed because of the high vibration environment which would cause excessive wiper noise and possibly even potentiometer failure. Fixed discrete balance resistors were also determined to be unacceptable because of the tremendous number of 73-2C screened resistors values that would have to be stocked to cover the bridge unbalances that could be expected; Logistically it was impractical. As indicated by Figure 22, passively trimmed thick film resistors were chosen for the balance resistors. The range (span) was accomplished by a discrete resistor in which the calculated value, ±10% and ±20% or a total of 5 was stocked for each bridge. It is these resistors that are used for setting (adjusting) the channel gain by controlling the bridge excitation voltage. The gain of all 10 bridge amplifiers is preset at the factory. The first stage gain is 102, the second stage varies from 4 to 28. The resultant gains versus loads are shown by Figure 23. The individual thick film resistor networks are initially 3K ohms, capable of being trimmed to 150K ohms. The thick film resistors were prepared from the same ink batch so as to minimize temperature effects from the voltage divider. During initial load cell integration testing, the thick film circuit card is removed from the SCU and replaced with an extender card attached to a test box that is configured to an identical circuit equipped with potentiometers for each of the thick film resistors. The flight load cells are balanced for correct offset followed by full scale loads being applied. The span potentiometer is set to one of the predetermined stocked select resistors that most nearly allows the full scale range to be achieved. Several repeated runs are performed and assuming repeatability is acceptable, the value of each potentiometer is measured (out of circuit) and recorded. The thick film resistors are trimmed to within ±0.5% of the recorded value, the range resistor installed, the assembly installed in the SCU and final calibration accomplished as follows.

Each nosetip load sensor, as shown in Figure 24, was individually calibrated by applying known incremental loads on an assembled nosetip in known, controlled directions, Calibration coefficients were generated which was used to reduce flight data.

Calibrations were performed by installing the sensors into the forward vehicle frustum and mounting the assembly in a rigid structure which is equipped with aligned force applications and measuring devices. The axial and radial forces are applied with hydraulic jacks which are manually controlled. The magnitude of the applied loads are measured with precision (0.1%) load cells. The loads are applied to the load sensor through a loading head that mates with an aluminum plug which simulates the carbon-carbon nosetip. The calibrations fixture includes provisions for rotating the sensor relative to the line of radial force applications. The sensor strain gage bridge circuits are connected to the SCU whose output is recorded on an SCU Test Set. The load cell outputs are read and recorded with a Doric Digital Printer and Monitor. The instrumentation and loading setups for calibrating the SCU and the nosetip load sensor are shown in Figure 25.

The accuracy requirement of 1 percent of full scale (5 volts) established for the load sensor necessitated a calibration procedure which accounts for non-linearity of data, crosstalk between lateral and axial forces and interaction between simultaneous applications of two loads.

The calibration for axial loading consisted of incrementing the applied axial load under constant lateral loading (0, 900, 1800 lbs.). This procedure was performed at a lateral load application of 0° roll angle. The calibration for lateral force involved incrementing the lateral force under constant axial loading (1800 and 3200 lbs.). This procedure was repeated at 25 different roll angles (increments varied from 10°, windward side, to 30°, leeward side). A schematic of the calibration data is shown in Figure 26.

The calibration data is reduced and combined through a computer program which generates a calibration matrix. The sensor flight data (sensor outputs, sensor temperatures, and vehicle accelerations, including spin and pitch rates) is input into the program (via tape) to determine values of force magnitudes, directions, and location. The program makes corrections to strain readings caused by temperature effects. The program also corrects the measured forces for inertia loads to obtain the aerodynamic forces on the nosetip. The program calculates the deflected shape of the nosetip (based on ground test calibration data) for input into the reduction of the nose recession sensor data.

The nomographs in Figure 27 depicts the procedure which is utilized by the computer program to reduce flight data. The magnitude of the axial loading is first determined by dividing the voltage change of the axial gages by a calibration coefficient based on the magnitude of the voltage change in the forward pitch gages (see nomograph No. 1). (The

aerodynamic axial load acting on the nosetip is obtained by correcting the measured axial force for the axial inertia loads.) After the magnitude of the flight axial force is determined, the program generates a new set of lateral load calibration curves based on the axial load value. The curves are generated by linearly interpolating between the calibration values of 1600 and 3200 lbs. These calibration curves are generated for each of the bending strain stations on the sensor, see Figure 27, nomograph No. 2. For the calculation of lateral load, the program takes the output signal of the pitch and yaw gages and establishes a vector which is compared to the vectors for all the data points on the calibration plot. The four calibration point vectors which bound the data point vector are thus determined. Once the boundary vectors are established, the bending moment and then the angle of the bending plane relative to the pitch plane is determined by linear interpolation between moment and angle values for each of the four calibration vectors, see Nomograph No. 3. The bending moments at each bending gage station are converted into pitch and yaw components prior to correcting for inertia effects. The difference in the bending moments divided by the distance (4 inches) gives the nosetip aerodynamic lateral load. The location of the aerodynamic lateral load is obtained by dividing the bending moment at the forward pitch gage by the magnitude of the aerodynamic lateral load.

The load sensor has performed extremely well in two AMaRV flight tests to date. Each flight has produced excellent data for determining the aerodymanic coefficients associated with an ablating nosetip. Figure 28 depicts the aerodynamic data from an actual AMaRV flight test and is typical of all data obtained. The figure illustrates the normal force coefficient measurement plotted against altitude and compared to predictions. It has demonstrated that the nosetip forces can be measured with a high degree of accuracy.

The AMaRV vehicle also contains a load sensor positioned at each end of the control surface hinges. This sensor measured shear strains at 90° intervals in a shaft which transfers control surface loads into the vehicle. The sensor has performed satisfactorily in two flights. The operation and/or design details cannot be shown due to security restrictions.

CONCLUSION

Instrumentation data recovered to date on FTV-1 and FTV-2 has been excellent. Vibration, shock and acoustic data recovered by merging short bursts of information has been quite successful. It has been demonstrated that through rather elaborate calibration and data reduction techniques, in-flight nose loads can be measured to extreme accuracies (±1%). Though the AMaRV reduced data has provided excellent results with few anomalies attributed to the instrumentation, it is apparent that the shear volume and frequency response demands of raw data is approaching saturation of the ground support station, not only at the factory, but at the launch facility and down-range receivers.

It is apparent, that as flight performance measurements become more demanding, not only in reliability and package size, but in frequency response (which means more bandwidths, hence increased bit rate, hence more RF power or additional transmitters, larger battery capacity, greater heat dissipation, more complex antenna subsystems and more volume), more and more on-board processing and data compression techniques will have to be devised that are acceptable to both system designers and experimenters.

ACKNOWLEDGEMENTS

References

1. Legendre, P. J.; Casranto, J. M.; Gragowsky, W. R.; and Fowler, R. C. “The Challenge of Re-Entry Instrumentation presented at the 24th ISA Instrumentation Symposium, Albuquerque, New Mexico, May 1-4, 1978.

2. Endsley, N. H.; Lee, H. K.; and Mashhoff, R. M. “A Data Acquisition System Featuring On-Board Processing” International Telemetry Conference (ITC) Volume XIII, pages 113-129, October 18-20, 1977.

3. Heller, H. H.; and Windall, S. C. “Dynamics of an Acoustical Probe for Measuring Pressure Fluctuations on a Hypersonic Reentry Vehicle” JASA, Volume 44, November 4, 1968.

4. O’Gara, M. R.; and McGunigle, R. D. “Aerodynamic Noise Spectrum and Acoustic Emission Measurements of Flight Nosetips, Using a Second Generation Ultrasonic Ablation Recession Gauge” presented at 22nd ISA Instrumentation Symposium, San Diego, Calif., May.25-27, 1976.

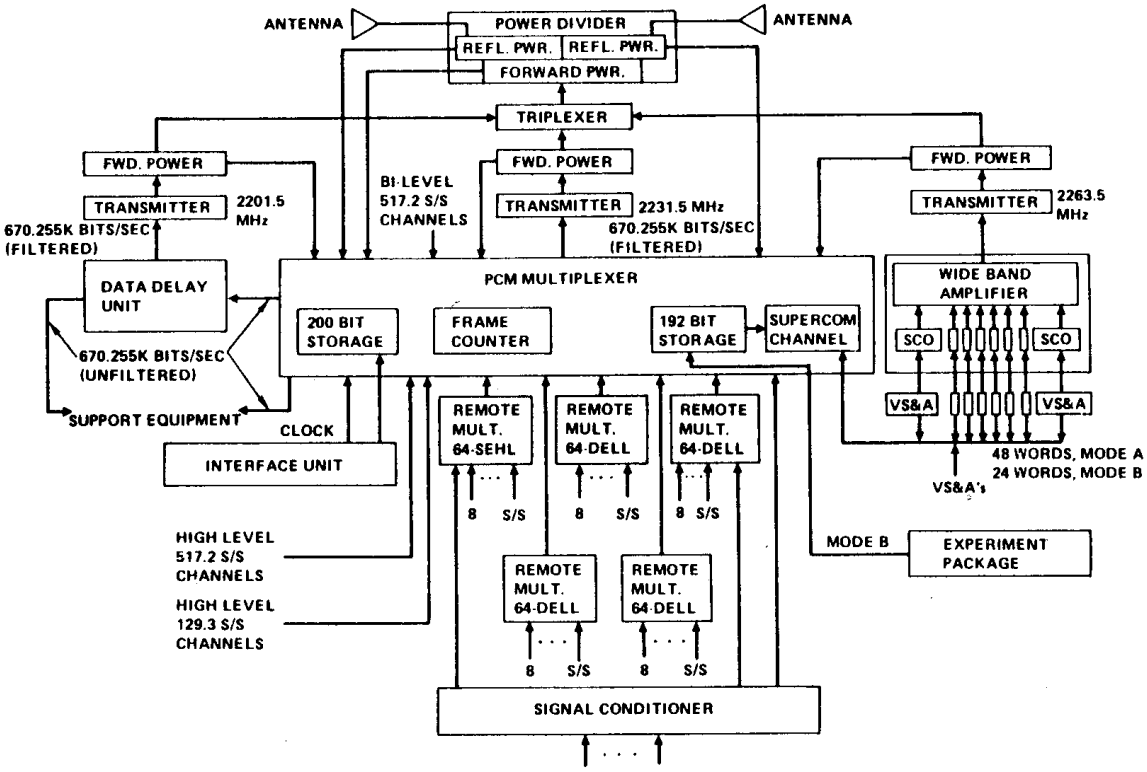

Figure 1. I&C Subsystem Block Diagram

COMPONENT SUBSYSTEM OR TECHNOLOGY	TOTAL PARAMETERS	BIT RATE USAGE
AA AND RMU	7	33,163
RIMU	30	78,768
CONTROL ACTUATION	17	52,016
LOAD CELL	9	18,576
NOSETIP RECESSION	7	448
AERO	223	14,272
VIBRATION AND ACOUSTICS	11	198,590
EP AND D	18	29,268
I AND C	15	960
RGC/IU	5	6,328
I/U SERIAL DIGITAL	400	103,400
		535,789
BIT SYNC, SUBFRAME I.D., FRAME COUNTER		16,549
PARITY		74,472
SPARES		43,445
TOTAL BIT RATE		670,255

Figure 2. Bit Rate Usage

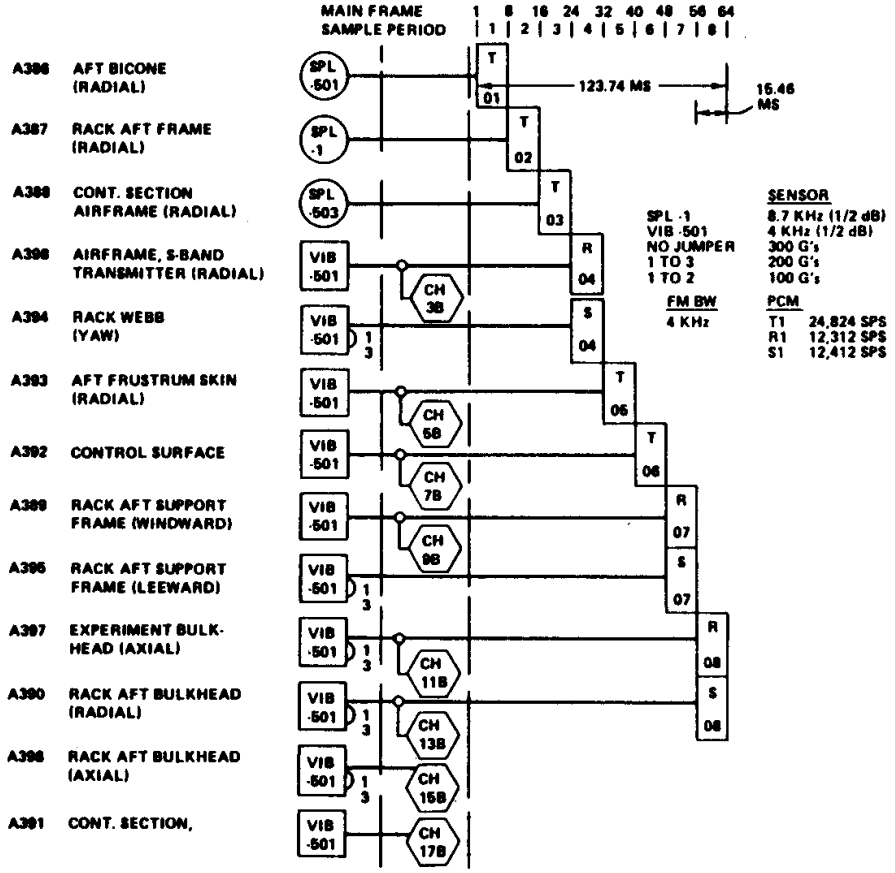

Figure 3. FTV-1 VS&A Channel Assignment

	Y1						Y2						Y3					
	X1	X2	X3	X4	X5	X6	X1	X2	X3	X4	X5	X6	X1	X2	X3	X4	X5	X6
Z1	S1	S2	S3/ID	SCA	SD	SCA	B1	SD	SCA	A1	SD	SCA	A2	A3	SCA	B2	E1	SCA
Z2	A4	A5	SCA	A6	SD	SCA	B3	SD	SCA	A7	SD	SCA	A8	A9	SCA	B4	A10	SCA
Z3	A11	A12	SCA	A13	SD	SCA	B5	SD	SCA	A14	SD	SCA	A15	A16	SCA	B6	E2	SCA
Z4	A17	A18	SCA	A19	SD	SCA	B7	SD	SCA	A20	SD	SCA	A21	A22	SCA	B8	A23	SCA
Z5	A24	A25	SCA	A26	SD	SCA	B9	SD	SCA	A27	SD	SCA	A28	A29	SCA	B10	E3	SCA
Z6	A30	A31	SCA	A32	SD	SCA	B11	SD	SCA	A33	SD	SCA	A34	A35	SCA	B12	A36	SCA
Z7	A37	A38	SCA	A39	SD	SCA	B13	SD	SCA	A40	SD	SCA	A41	A42	SCA	B14	SD	SCA
Z8	A43	A44	SCA	A45	SD	SCA	B15	SD	SCA	A46	SD	SCA	A47	A48	SCA	B16	FID	SCA

S	SYNC WORD	2	517.17 SPS	2
S/ID	3 BITS SYNC + 6 BITS ID	1	517.17 SPS	1
SCA	SUPERCOMMUTATOR MUX (11 ANALOG H.L. INPUTS)	11	24,824.16 SPS	48
SD	SERIAL DIGITAL (200 BITS)	25	517.17 SPS	25
A	H.L. ANALOG (ARRANGED FOR EXT CROSS STRAPPING)	48	517.17 SPS	48
B	H.L. ANALOG	64	129.29 SPS	16
E	BILEVEL	3	517.17 SPS	3
FID	FRAME COUNTER	1	517.17 SPS	1
				144

Figure 4. Mode A Format

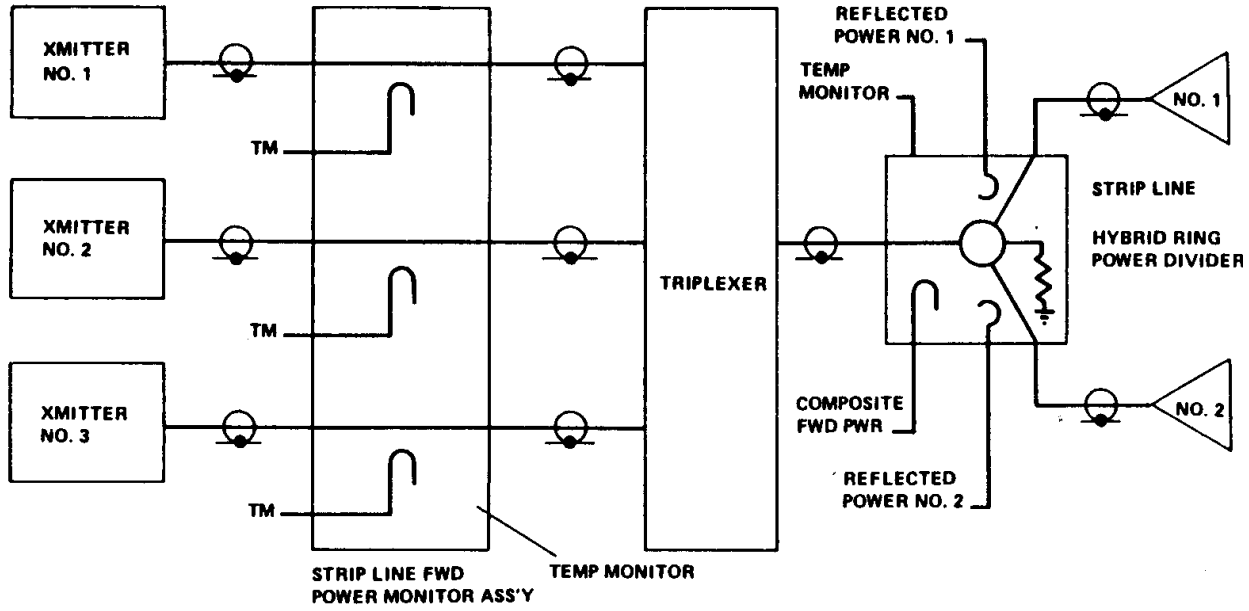

Figure 5. RF Subsystem

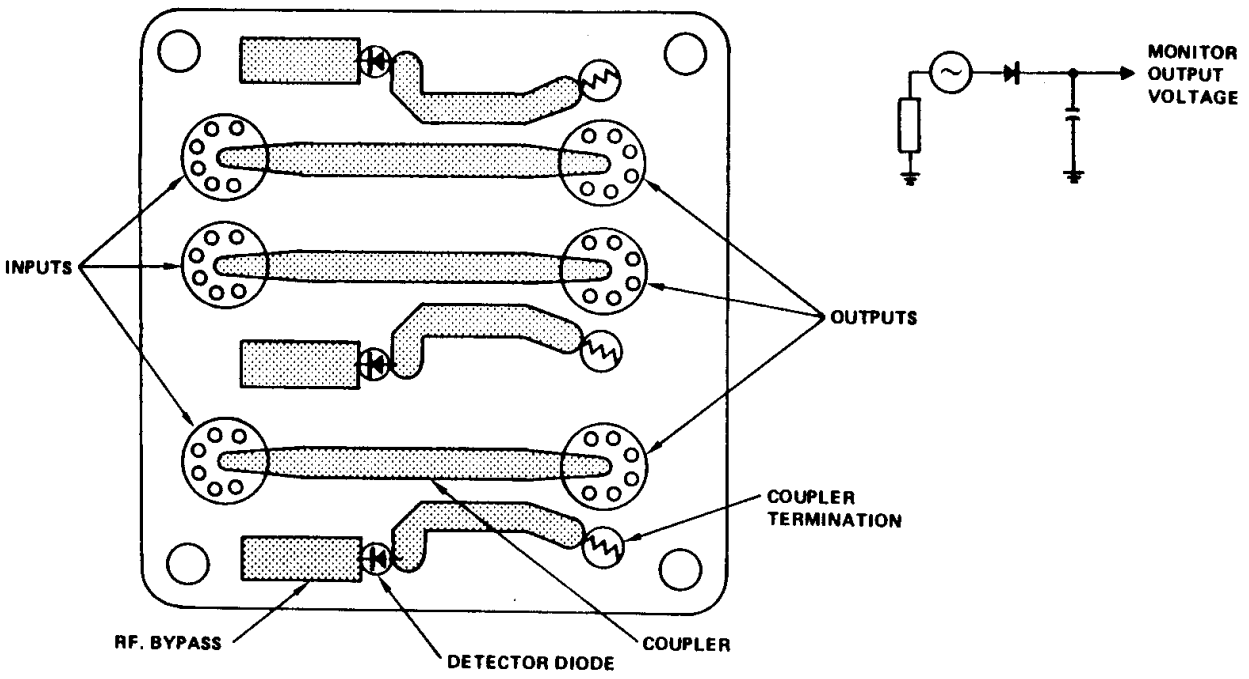

Figure 6. 3 Channel S-Band Power Monitor

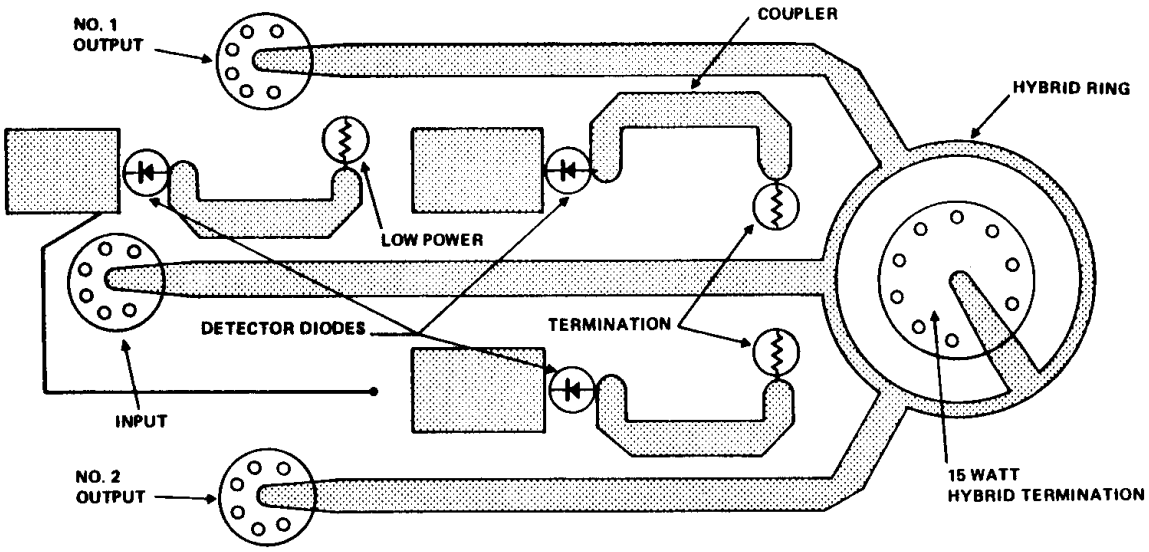

Figure 7. S-Band Power Divider/Monitor

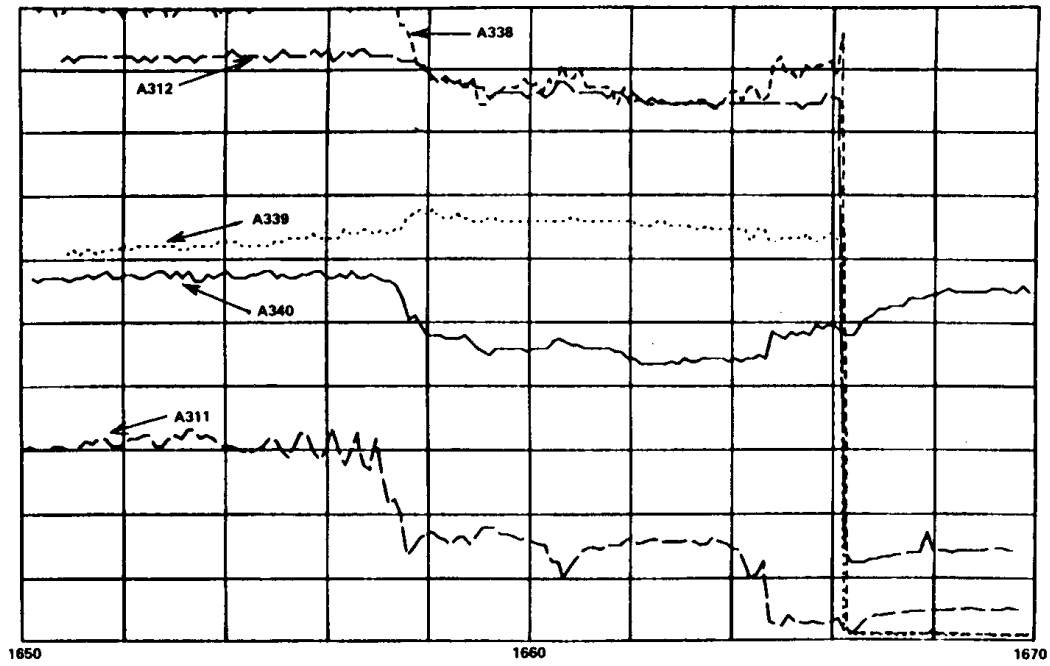

A340	FWD POWER XMITTER PCM	0.0000 - 10.00 WATTS
A339	FWD POWER XMITTER DDU	0.0000 - 10.00 WATTS
A338	FWD POWER FM XMITTER	0.0000 - 10.00 WATTS
A311	REFLECTED POWER ANT NO. 1	0.0000 - 20.00 WATTS
A312	FORWARD POWER PWR DVDR	0.0000 - 30.00 WATTS

Figure 8. Flight Results, RF Subsystem

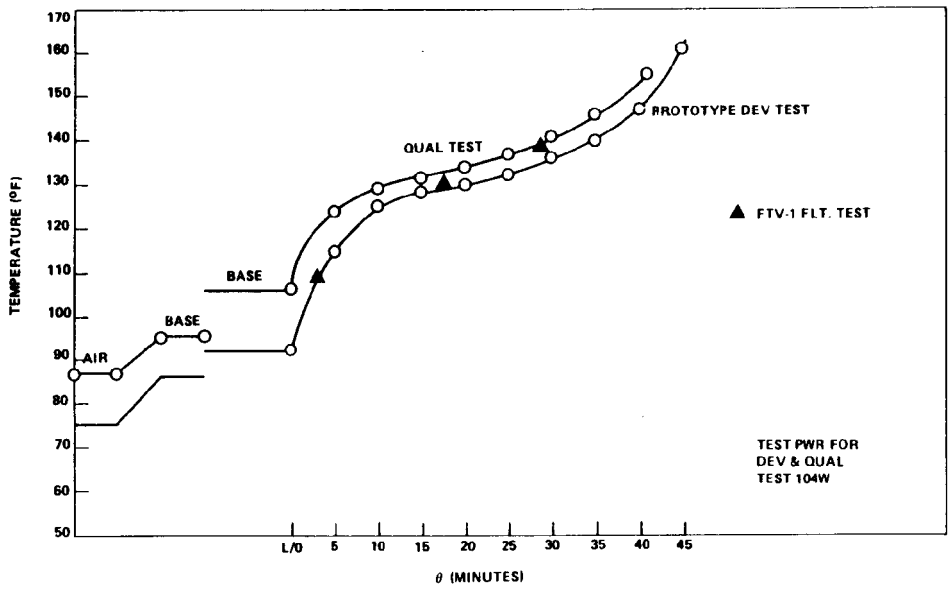

Figure 9. Transmitter Temperature Response

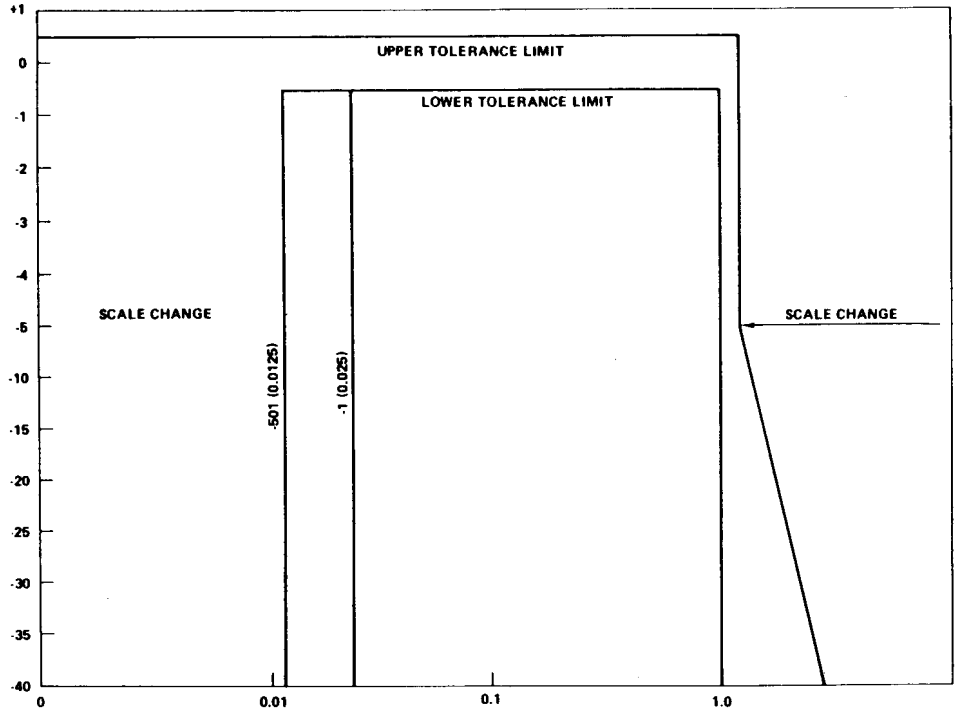

Figure 10. Normlized Frequency Response Curve

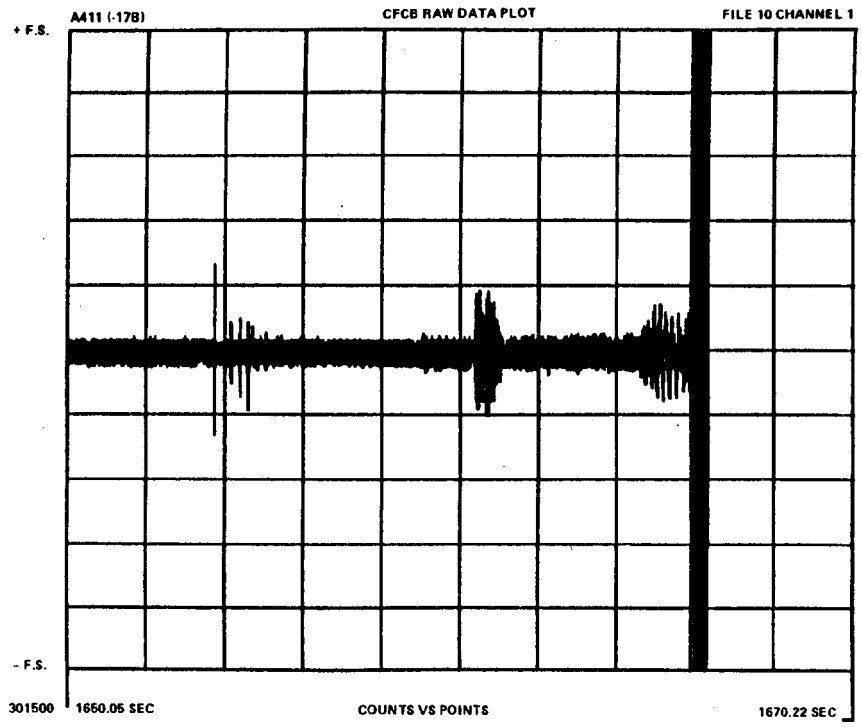

Figure 11. A411 (-17B) CFCB Raw Data Plot File 10 Channel 1

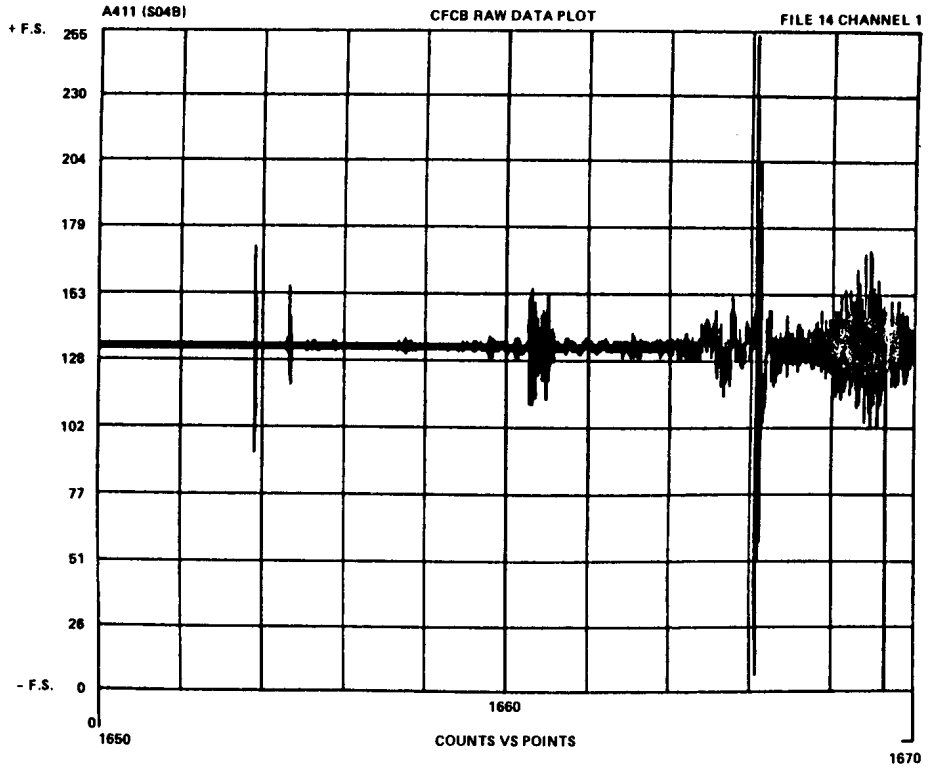

Figure 12. A411 (SO4B) CFCB Raw Data Plot File 14 Channel 1

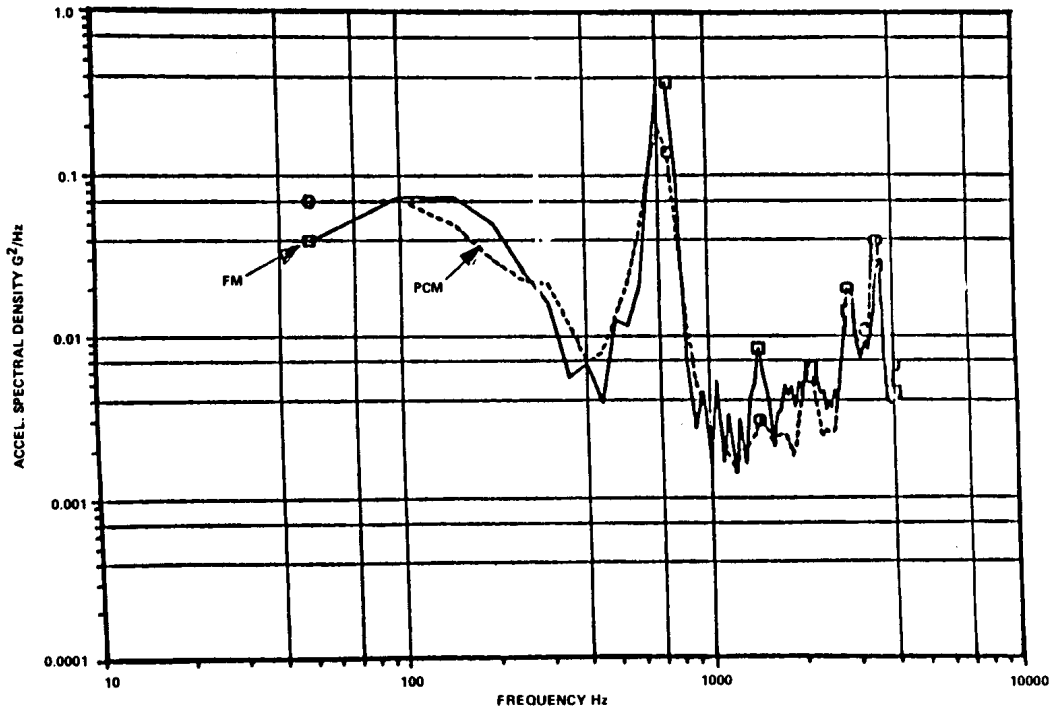

Figure 13. FM vs PCM Control Surface Vibration Spectrum at T ± 1680 sec

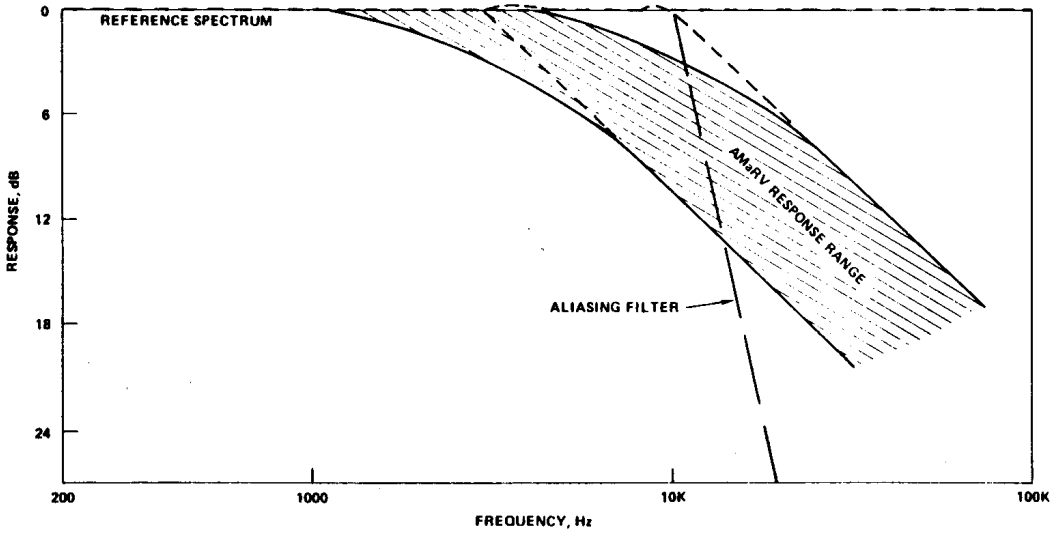

Figure 14. K-West Model 398 Acoustic Sensor Frequency Response to Pressure Fluctuations in a Hypersonic Flow Field

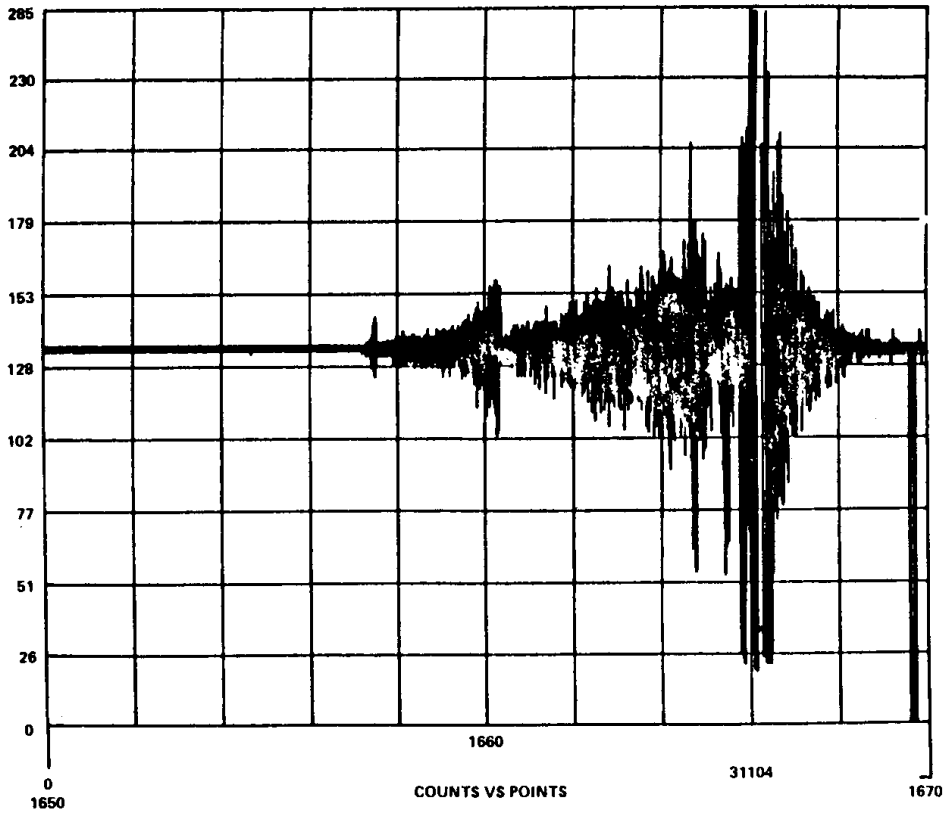

Figure 15. A400 CFCB Raw Data Plot File 5 Channel 1

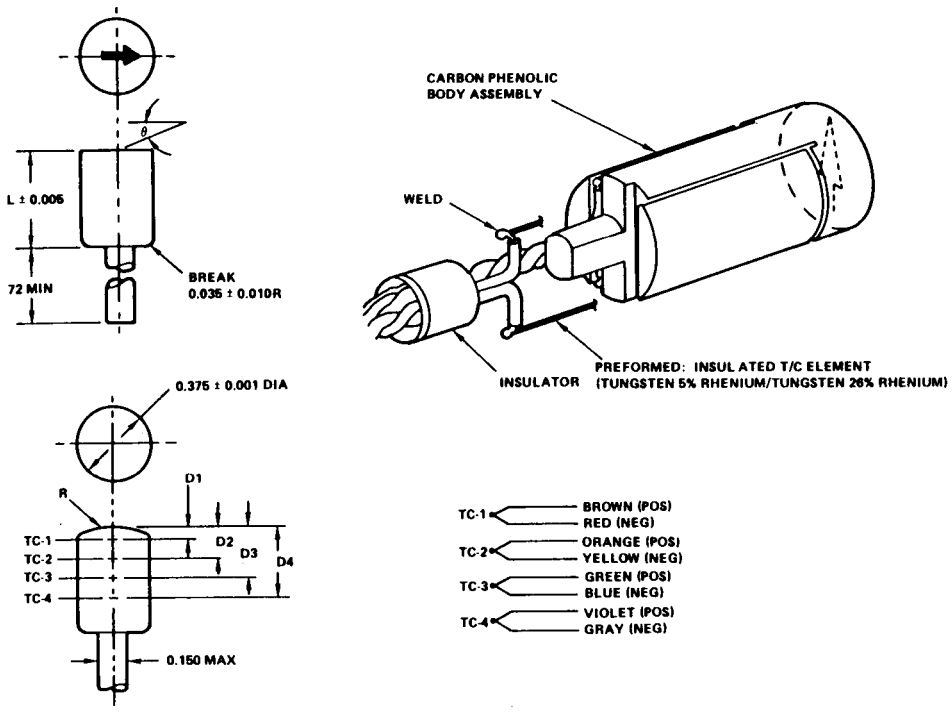

Figure 16. In-Depth Thermocouple Plug

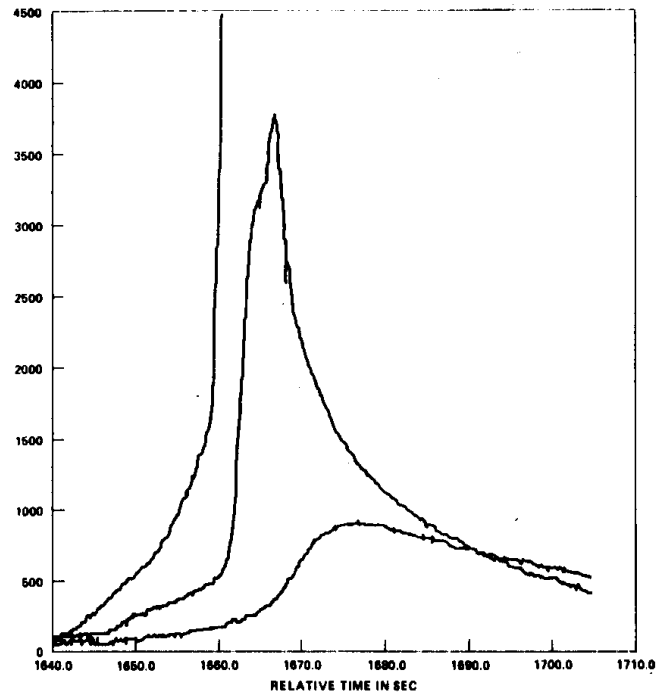

MEAS. NUMBER	CHANNEL ASGN.	TITLE	RANGE	UNITS	GRID SYS
A118	F-128-18	HTSHLD TEMP IDT-11(32.6/90/0.01)	0 TO 4500	DEG F	AA
A119	F-128-19	HTSHLD TEMP IDT-11(32.6/90/0.08)	0 TO 4500	DEG F	AB
A120	F-128-08	HTSHLD TEMP IDT-11(32.6/90/0.20)	0 TO 4500	DEG F	AC

Figure 17. FTV-02 Re-entry Plot No IDT-11

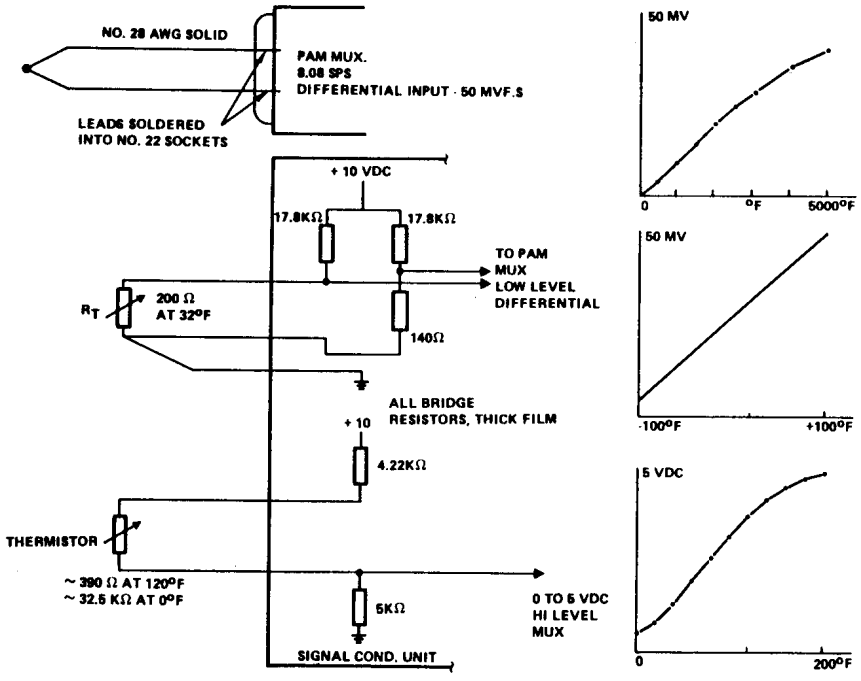

Figure 18. Thermal Sensor Wiring Configuration and Voltage Output

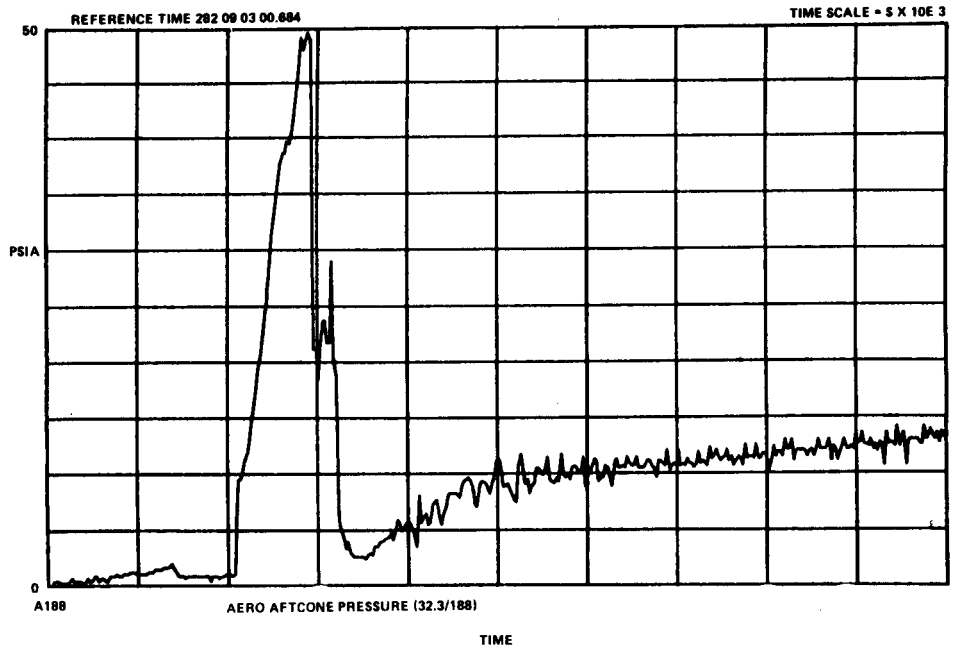

Figure 19. Tape ID=ANA Test ID=4900005 Test Site - 100880

Figure20. Flowmeter Signal Conditioning

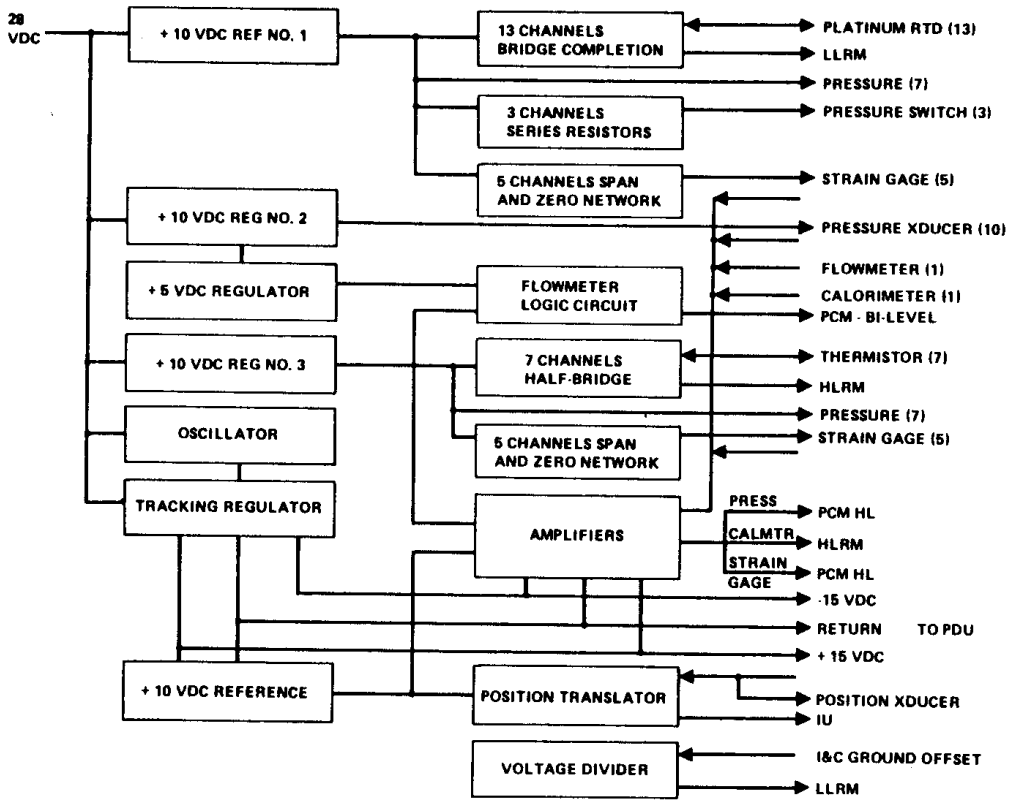

Figure 21. SCU Block Diagram

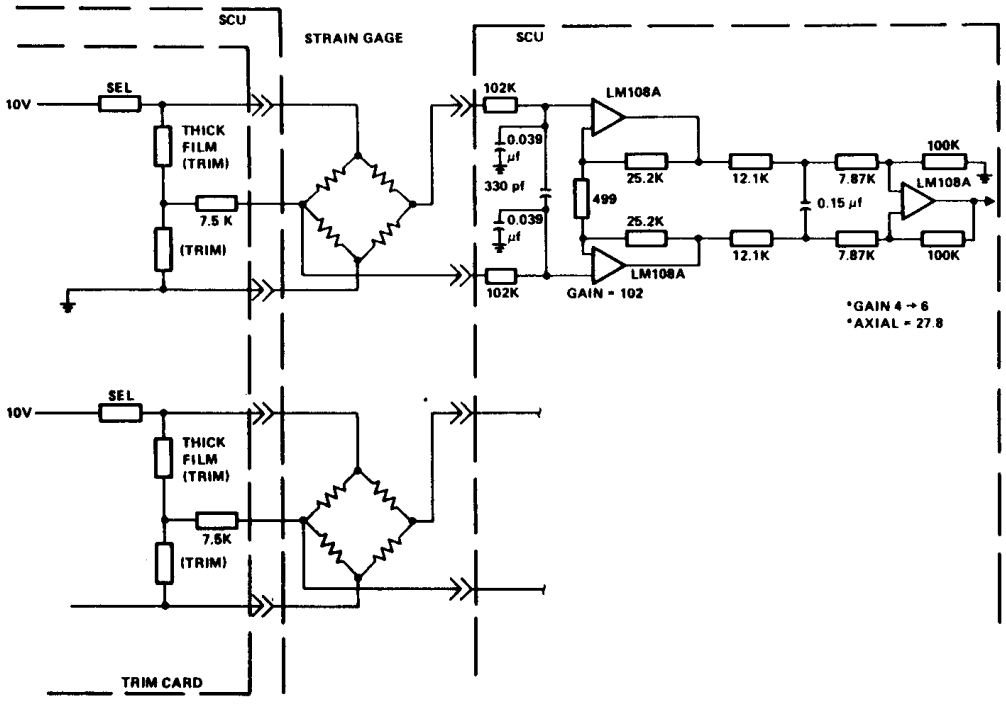

Figure 22. Strain Gage Circuit

MEAS. NO.	TITLE	LOAD (LBS)	SIGNAL GAIN	-3dB BANDWIDTH (Hz)	SAMPLE RATE (SPS)
A053	STRAIN, HINGE	-738 TO +1771	648	40	258
A054	STRAIN, HINGE	-1424 TO +1430	510	40	258
A055	STRAIN, HINGE	-748 TO +1803	648	40	258
A056	STRAIN, HINGE	-1587 TO +1612	510	40	258
A074	STRAIN, NOSE LOADS, PITCH	-1168 TO +1828	648	40	258
A075	STRAIN, NOSE LOADS, PITCH	-2532 TO +2972	510	40	258
A076	STRAIN, NOSE LOADS, YAW	-1092 TO +1089	843	40	258
A077	STRAIN, NOSE LOADS, YAW	±1822	648	40	258
A078	STRAIN, NOSE LOADS, AXIAL	-120 TO +7868	2820	40	258

Figure 23.SCU Strain Gap Conditioning Circuit Design

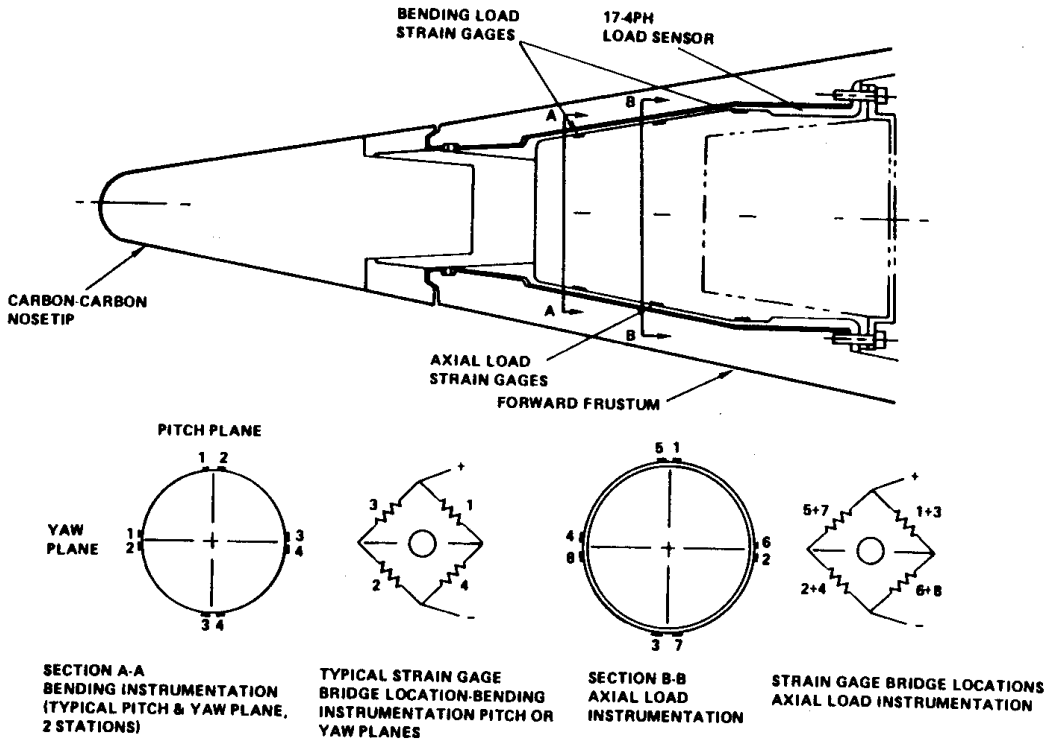

Figure 24. Nose Load Sensor Configuration

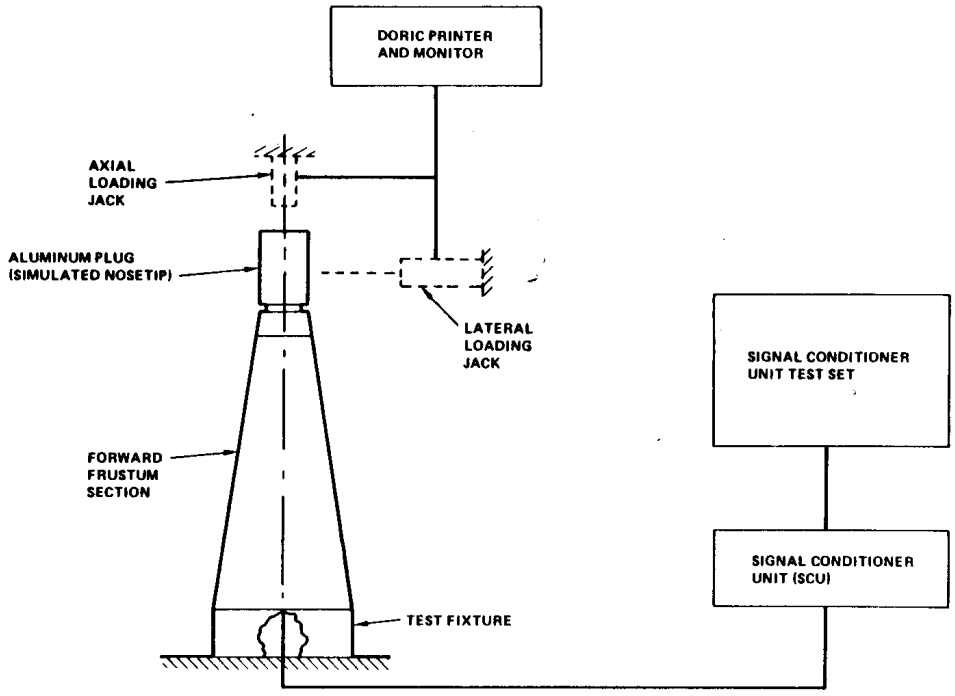

Figure 25. Test Setup for SCU and Nosetip Load Sensor Calibration

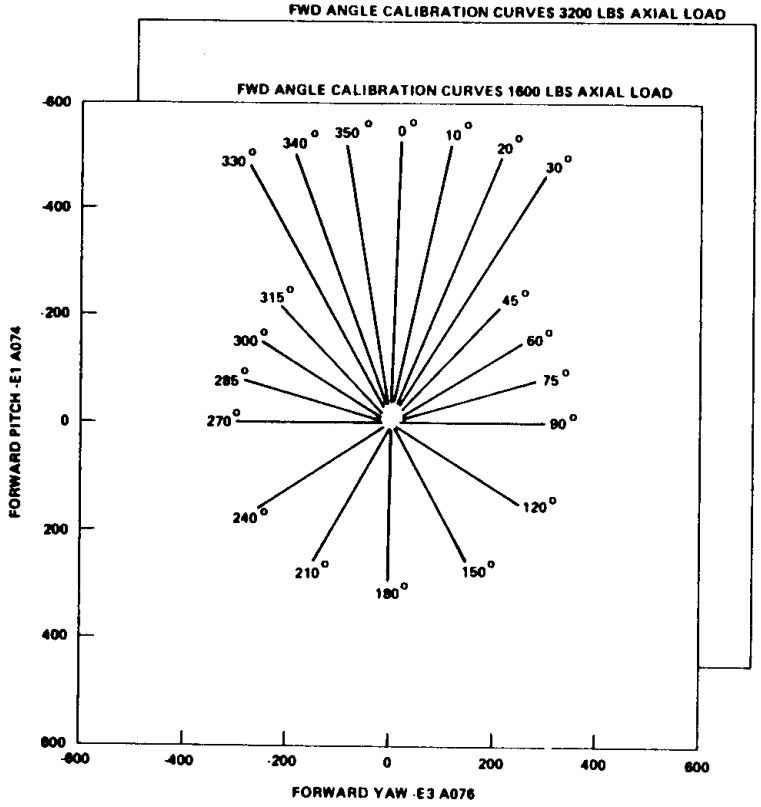

Figure 26. Typical Calibration Curves at Constant Axial Load

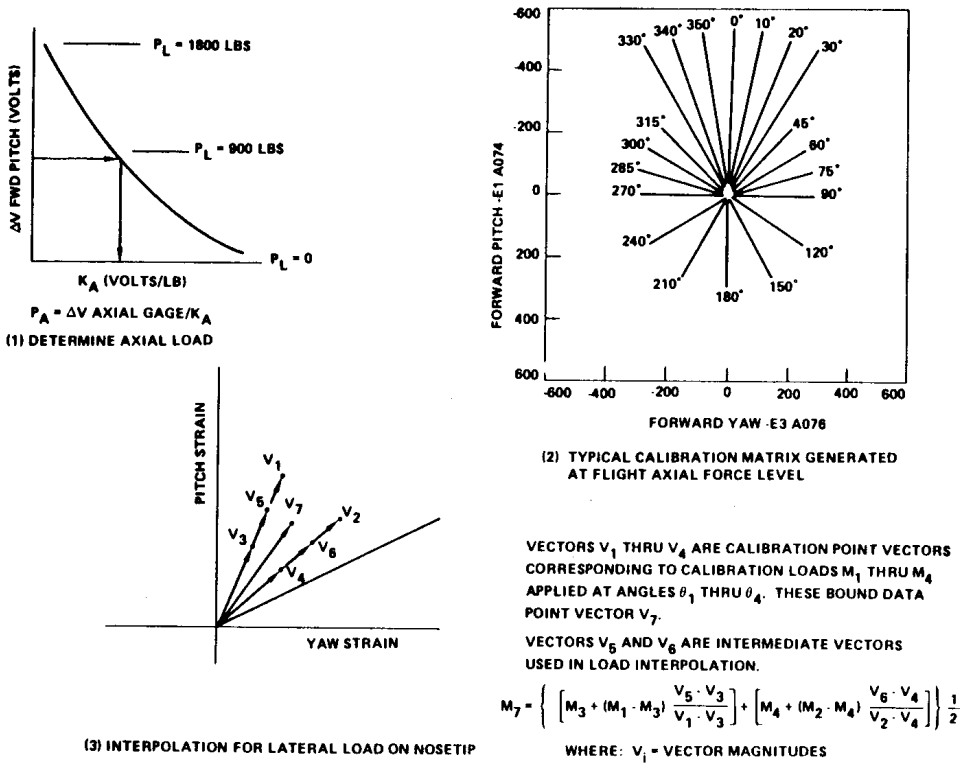

Figure 27. Nomographs Depicting Operation of Computer Program to Reduce Flight Data

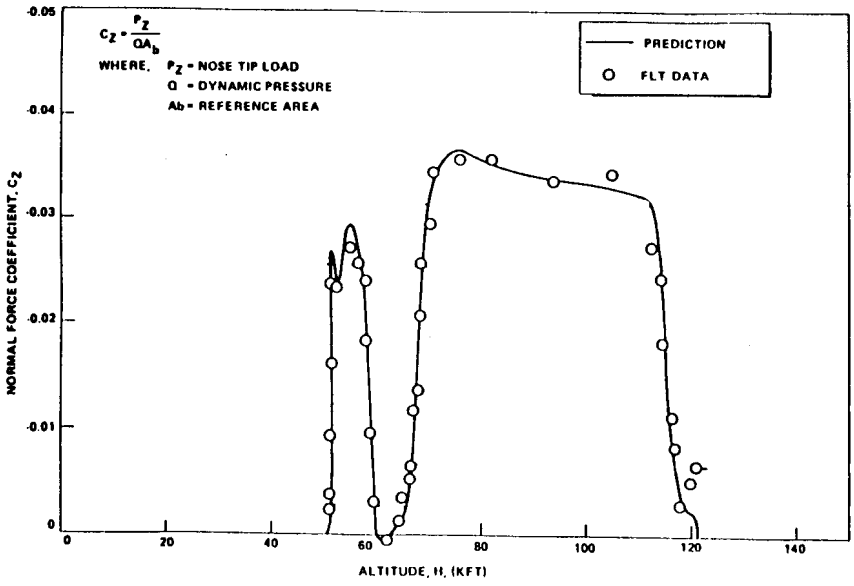

Figure 28. Normal Force Coefficient Comparisons Along Flight Trajectory